Influence of B/N co-doping on electrical and photoluminescence properties of CVD grown homoepitaxial diamond films

OPEN ACCESS
IOP Publishing
Nanotechnology

Nanotechnology **33** (2022) 125603 (16pp)
https://doi.org/10.1088/1361-6528/ac4130

Influence of B/N co-doping on electrical and photoluminescence properties of CVD grown homoepitaxial diamond films

Srinivasu Kunuku[1], Mateusz Ficek[1], Aleksandra Wieloszynska[1], Magdalena Tamulewicz-Szwajkowska[2], Krzysztof Gajewski[2], Miroslaw Sawczak[3], Aneta Lewkowicz[4], Jacek Ryl[5], Tedor Gotszalk[2] and Robert Bogdanowicz[1]

[1] Department of Metrology and Optoelectronics, Faculty of Electronics, Telecommunications and Informatics, Gdańsk University of Technology, 11/12 Narutowicza St., 80-233, Gdańsk, Poland
[2] Department of Nanometrology, Wrocław University of Science and Technology, Janiszewskiego 11/17 St., 50-372, Wrocław, Poland
[3] The Szewalski Institute of Fluid-Flow Machinery, Polish Academy of Sciences, 80-231, Gdansk, Poland
[4] Institute of Experimental Physics, Faculty of Mathematics, Physics and Informatics, University of Gdansk, Wita Stwosza 57, 80-952 Gdansk, Poland
[5] Institute of Nanotechnology and Materials Engineering, Gdansk University of Technology, Narutowicza 11/12, 80-233 Gdansk, Poland

E-mail: rbogdan@eti.pg.edu.pl

Received 26 September 2021, revised 1 December 2021
Accepted for publication 8 December 2021
Published 28 December 2021

Abstract

Boron doped diamond (BDD) has great potential in electrical, and electrochemical sensing applications. The growth parameters, substrates, and synthesis method play a vital role in the preparation of semiconducting BDD to metallic BDD. Doping of other elements along with boron (B) into diamond demonstrated improved efficacy of B doping and exceptional properties. In the present study, B and nitrogen (N) co-doped diamond has been synthesized on single crystalline diamond (SCD) IIa and SCD Ib substrates in a microwave plasma-assisted chemical vapor deposition process. The B/N co-doping into CVD diamond has been conducted at constant N flow of N/C $\sim$ 0.02 with three different B/C doping concentrations of B/C $\sim$ 2500 ppm, 5000 ppm, 7500 ppm. Atomic force microscopy topography depicted the flat and smooth surface with low surface roughness for low B doping, whereas surface features like hillock structures and un-epitaxial diamond crystals with high surface roughness were observed for high B doping concentrations. KPFM measurements revealed that the work function (4.74–4.94 eV) has not varied significantly for CVD diamond synthesized with different B/C concentrations. Raman spectroscopy measurements described the growth of high-quality diamond and photoluminescence studies revealed the formation of high-density nitrogen-vacancy centers in CVD diamond layers. X-ray photoelectron spectroscopy results confirmed the successful B doping and the increase in N doping with B doping concentration. The room temperature electrical resistance measurements of CVD diamond layers (B/C $\sim$ 7500 ppm) have shown the low resistance value $\sim$9.29 Ω for CVD diamond/SCD IIa, and the resistance value $\sim$16.55 Ω for CVD diamond/SCD Ib samples.

Keywords: boron/nitrogen co-doped diamond, homoepitaxial, nitrogen-vacancy, activation energy

(Some figures may appear in colour only in the online journal)

1. Introduction

Diamond is one of the semiconductors, exhibits unique properties like high thermal conductivity, chemical inertness, high mechanical hardness, wide bandgap, low dielectric constant, high breakdown field, high hole mobility, and tunable negative electron affinity. Combination of these exceptional properties drives the diamond into a variety of applications like electron field emitters, single-photon sources, biological and chemical sensors, microelectromechanical devices, hard coatings, heat sinks, and high power electronics [1–4]. Diamond is a wide-bandgap material, which enables to introducing the variety of impurities into bandgap to tuning the electrical and optical properties. The insulating diamond could be converted to electrically conducting p-type by doping with boron (B) and n-type diamond by nitrogen (N) or phosphorus (P) doping [5]. In addition, doped impurities like boron, nitrogen, silicon, and nickel lead to the formation of boron-vacancy (BV), nitrogen-vacancy (NV), silicon-vacancy (SiV), and nickel-vacancy (NiV) kind of diamond color centers, which are emerging as single-photon sources for quantum computing and quantum information processing, bioimaging, and low magnetic field sensor applications [6–10].

B is a substantial dopant element for the synthesis of p-type diamond because B acts as an acceptor in the diamond lattice thus boron-doped diamond (BDD) is a prominent material for electro- chemistry due to its low carrier activation energy ~0.37 eV, wide potential window, and low-background current [11]. Hence, BDD electrodes were employed in several promising applications like electrochemical sensing [12–14], electron field emission devices [15], wastewater treatment [16], and electrodes for the construction of supercapacitors [17, 18]. The B doping concentration in insulating diamond defines its ability of conductivity, for instance at the doping concertation of $\sim 10^{18}$ cm^{-3} the insulating diamond transforms to semiconducting diamond [19], whereas insulating diamond converts to metallic at the B doping concentration above 10^{21} cm^{-3} [20]. However, the high doping of B causes the degradation of the crystalline quality of the diamond and around 10 % of doped B atoms could not act as acceptors [21, 22]. Moreover, B doping is most effective and has shown higher conductivity in large diamond crystals (microcrystalline diamond) than in smaller nanodiamond grains [23]. Therefore, the efficiency of B doping and related properties in single-crystalline diamond (SCD) are deciphering subjects for conducting research.

In addition, the co-doping of two elements into diamond has demonstrated superior properties compared to single element doping. High quality and low stress gem-SCD crystals with high N concentrations have been prepared by co-doping of N and hydrogen (H) into diamond in the high-pressure high-temperature (HPHT) method [24]. B and sulfur (S) co-doped diamond synthesized in HPHT process exhibited n-type conductivity, and the addition of B enhanced the S doping into diamond compared to single S doped diamond [25]. B/H co-doped HPHT grown SCD samples showed p-type conductivity with high carrier concentration and high conductivity than B-doped diamond [26]. Theoretical studies of B/N co-doped diamond have been demonstrated with n-type conductivity and enhanced N doping efficiency by the addition of B, B boosts the solubility limit of N in diamond and decreases the lattice-relaxation energy [27]. Green diamond crystals (nearly transparent) have been synthesized by B/N co-doping into diamond using the HPHT process, which illustrated the inhibition of N precipitation by increasing the N solubility in the diamond [28]. The N-rich B doped HPHT diamond samples have revealed a better crystalline quality with increasing addition of B due to B–N formation, p-type conductivity, and low Hall mobility due to scattering occurred by N defects in the diamond lattice [29].

Karna *et al* synthesized B/N co-doped SCD samples on Ib substrates at relatively high nitrogen doping levels demonstrating enhanced growth rate with non-epitaxial growth of doped diamond [30] . In addition, they manifested that increase of N doping level induces the decrease in electrical conductivity, whereas does not reported the photoluminescence properties of grown samples [30]. Issaoui *et al* reported the use of B/N co-doping for application in vertical power electronic components showing that nitrogen admixture allowed for compensation of the strain induced by boron incorporation in single crystal diamond [31]. The B/N co-doped diamond films have been demonstrated by Guo *et al* as electrodes with enhanced electrochemical performance when compared with standards BDD [32–34]. This effect was attributed to the enrichment of CO groups and the increased concentrations of sp^2 phases in the co-doped films, what allows for enhanced performance in electroanalytical applications [32].

Synthesis of high-quality NV center-diamond on HPHT SCD substrates are attracting towards device fabrication in quantum sensing applications [35]. The charge state control of NV center is very crucial parameter for utilizing them in quantum sensing applications [35, 36]. The boron presence in NV center-diamond has been demonstrated the passive charge state control of NV center by tuning towards NV° due to its acceptor nature [37]. However, nitrogen related optical features have been not achieved for lightly B doped CVD diamond [38]. Therefore, influence of B concentration on the formation of NV centers in CVD process is an ambiguous topic for investigation. Next, the electrical and NV emission properties of B/N co-doped CVD diamond/SCD substrates is a prime subject in development of quantum and electrochemical sensor applications. Therefore, in the present study, B/N co-doped CVD diamond has been overgrown on SCD IIa and SCD Ib substrates using the microwave

plasma-assisted chemical vapor deposition (MPACVD) process. Three different B/N co-doped CVD diamond samples have been synthesized by the addition of B/C $\sim$ 2500 ppm, 5000 ppm, and 7500 ppm, with the inclusion of a constant N_2 flow at 0.12 SCCM (N/C $\sim$ 0.02) into growth plasma. Surface topography of CVD diamond layers has been investigated using atomic force microscopy (AFM), and Kelvin probe force microscopy (KPFM) was employed to measure the contact potential difference (CPD) to calculate the work function of these CVD diamond layers. Photoluminescence (PL) spectra of all these CVD diamond/SCD substrates were obtained to examine the influence of high B doping in the NV center's formation and their emission characteristics. Electrical resistance measurements were carried out at different temperatures $\sim$77 to 573 K to investigate the influence of temperature on electrical resistance and estimation of activation energy (E_a) of the B/N co-doped CVD diamond layers. X-ray photoelectron spectroscopy measurements were carried out for investigation on B/N doping efficacy and its influence on diamond quality.

2. Experimental methods

B/N co-doped diamond overgrown on the HPHT-SCD substrates using a MPACVD system (2.45 GHz, Seki Technotron AX5400S, Japan). Here, two types of SCD substrates have been utilized to grow the B/N co-doped diamond, i.e. SCD IIa (3 $\times$ 3 $\times$ 0.5 mm; New Diamond Technologies, Russia), and SCD Ib (3 $\times$ 3 $\times$ 1.0 mm). SCD IIa consists of the impurity levels of N $<$10 ppb and B $<$50 ppb, whereas the SCD Ib substrate has the impurity levels of N $<$1 ppm and B $<$0.05 ppm. Both the SCD IIa and Ib substrates have consisted of (100) face orientation and edge orientation of (110). Prior to the growth of B/N co-doped diamond, SCD substrates were cleaned by the RCA process. Afterward, RCA-cleaned SCD substrates were placed in the MPACVD chamber and then subjected to H-plasma to clean the surface. The H-plasma surface cleaning has been performed with a H_2 flow rate of 600 SCCM, working pressure of 100 Torr, microwave power of 1000 kW, substrate temperature of 900 °C, and process time of 10 min (table 1). B/N co-doping was executed using diborane (B_2H_6) and N_2 gases as dopant precursors. Three kinds of B/N co-doped diamond samples were prepared by [B]/[C] concentrations of 2500 ppm, 5000 ppm, and 7500 ppm with a fixed N/C $\sim$ 0.02. B/N co-doped diamond samples were grown using CH_4 $\sim$ 12 SCCM, H_2 $\sim$ 600 SCCM, microwave power $\sim$ 1300 kW, pressure $\sim$ 100 Torr, substrate temperature $\sim$ 900 °C, and growth time of 30 min (table 1).

Subsequently, B–N co-doped diamond/SCD samples were annealed in a vacuum at 800 °C for 2 h. The high-temperature annealing process leads to the formation of graphite and oxide layers on the surface. Therefore, the annealed SCD samples were cleaned using H_2SO_4:HNO_3 (1:1) at 200 °C for 2 h, after that rinsed in DI water and dried in air. The surface topography of B/N co-doped diamond/SCD samples was observed by AFM. KPFM measurements were conducted using a Veeco/Bruker Nanoman V microscope equipped with a Nanoscope V controller for attaining the work function of the B–N doped diamond/SCD samples. To perform the KPFM measurements to measure the CPD, the surface of the B/N doped diamond/SCD samples was grounded using electrically conductive silver paint (Silver Conductive Adhesive 503, Electron Microscopy Sciences). CPD results were attained using the lift mode (two-pass technique), where each line must be scanned twice, the first tapping mode allows to observe the topography of the surface, and the second one is performed at a certain distance (lift-up height) from the sample surface, resulting in the measurement of a surface charge or the CPD. In the present study, the typical lift-up height of $\sim$50–150 nm was maintained to avoid unintentional contact of the scanning tip with the sample. Nanoworld ARROW-EFM probes with a typical spring constant of 2.8 N m^{-1} and resonant frequency of 75 kHz and silicon tips with a tip radius of 25 nm on a silicon cantilever with PtIr5 coating were used for scanning. The CPD of the sample was estimated from the CPD histogram taken from the whole scanned area. The work function of the samples was calculated based on the calibration using a highly oriented pyrolytic graphite (WF $\sim$ 4.6 eV).

Furthermore, polarization microscopy was utilized to observe the dislocations and strain in the CVD-grown B/N doped diamond layer on SCD substrates. The surface morphology of the B/N doped diamond was observed using a Keyence VHX-6000 3D digital microscope. Birefringence photographs of the CVD layers were taken with an OPTA-TECH LAB 40 POL microscope. Raman and photoluminescence (PL) spectroscopy measurements of the B/N co-doped diamonds samples were performed using a Horiba Jobin Yvon T64000 spectrometer equipped with three gratings (600, 1200, and 1800) system. The excitation source is a He–Cd (532 nm) laser with a power of 20 mW was focused on the B/N doped diamond/SCD samples using an Olympus MPFLN objective with 50$\times$ magnification. The PL measurements were carried out with a unique integration time of 5 s for all samples. X-ray photoelectron spectroscopy (XPS) measurements of the B/N doped diamond/SCD samples were measured using an Escalab 250Xi spectroscope (Thermo Fischer Scientific, UK) with a monochromatic Al Kα source. XPS measurements were conducted only for the B/C $\sim$ 2500 ppm and 7500 ppm of B/N doped diamond/SCD samples to check the success and influence of B/N doping into CDV diamond layers. The electrical resistivity of B/N co-doped diamond/SCD samples was measured at a low temperature of 77 K to a high temperature of 573 K by freezing and heating stage (THMS600, Linkam, UK), which was connected to a four-probe setup. Heating and freezing rates were maintained at a rate of 75 °C min^{-1}. THMS600 was connected to the measuring source unit (Keithley 2400, UK) and Arduino microcontroller, which is controlled by the program written in Python 2.7.2 software on a standard PC.

Table 1. Growth parameters of CVD diamond grown on SCD IIa and SCD Ib substrates.

CVD diamond	P (Torr)	H_2 (SCCM)	CH_4 (SCCM)	B_2H_6[a] (SCCM)	N_2 (SCCM)	T (°C)	Power (W)	Time (min)
B/N diamond/SCD IIa B/C ∼ 2500 ppm	100	600	0	0	0	900	1000	10
	100	600	12	7.5	0.12	900	1300	30
B/N diamond/SCD IIa B/C ∼ 5000 ppm	100	600	0	0	0	900	1000	10
	100	600	12	15	0.12	900	1300	30
B/N diamond/SCD IIa B/C ∼ 7500 ppm	100	600	0	0	0	900	1000	10
	100	600	12	22.5	0.12	900	1300	30
B/N diamond/SCD Ib B/C ∼ 2500 ppm	100	600	0	0	0	900	1000	10
	100	600	12	7.5	0.12	900	1300	30
B/N diamond/SCD Ib B/C ∼ 5000 ppm	100	600	0	0	0	900	1000	10
	100	600	12	15	0.12	900	1300	30
B/N diamond/SCD Ib B/C ∼ 7500 ppm	100	600	0	0	0	900	1000	10
	100	600	12	22.5	0.12	900	1300	30

[a] B_2H_6 is mixed in 2000 ppm of H_2 gas.

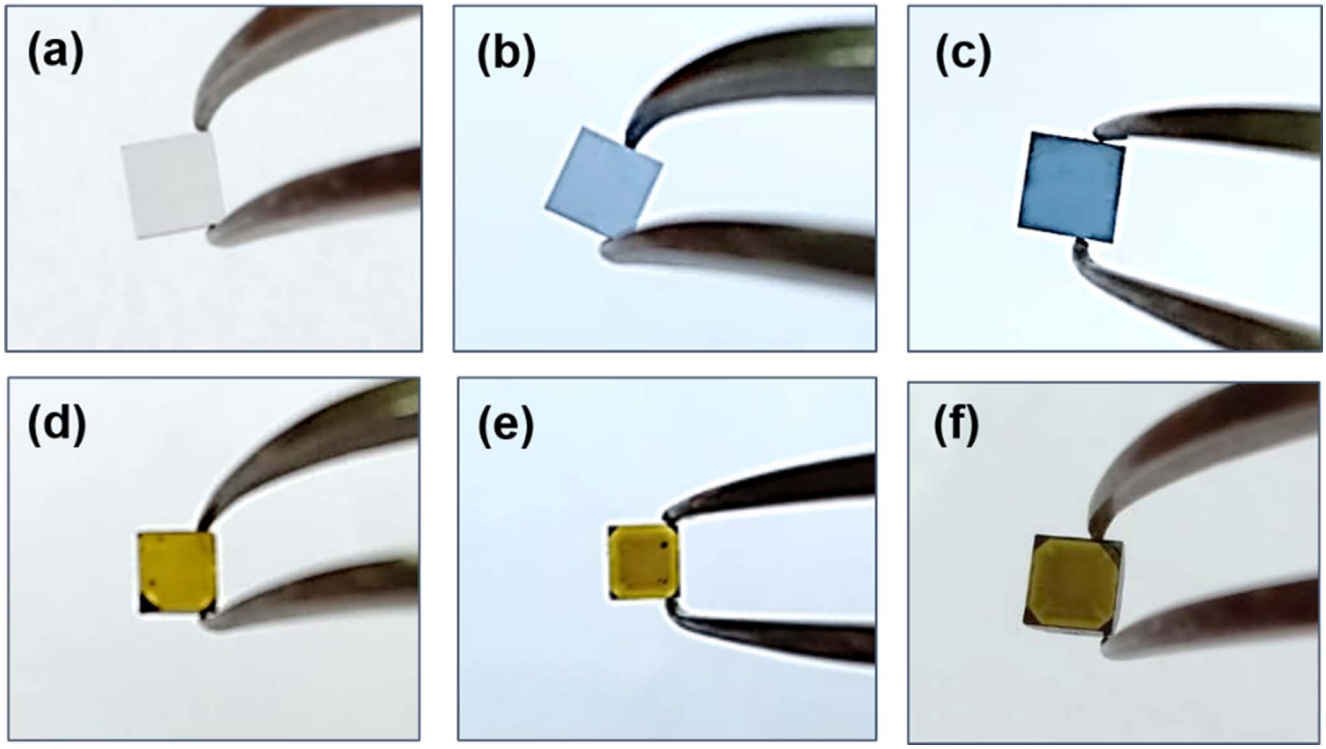

Figure 1. Photographs of B/N co-doped CVD diamond layer (with fixed N/C = 0.02) on SCD IIa; (a) B/C ∼ 2500 ppm (b) B/C ∼ 5000 ppm (c) B/C ∼ 7500 ppm, and photographs of B/N co-doped CVD diamond layer (with fixed N/C = 0.02) on SCD Ib; (d) B/C ∼ 2500 ppm (e) B/C ∼ 5000 ppm (f) B/C ∼ 7500 ppm.

3. Results and discussions

As-received SCD IIa substrates have appeared colorless due to lacking impurities, and as-received SCD Ib substrates appeared in yellow due to their intrinsic N impurities. Though, in the present study, B/N co-doping into CVD diamond (with various B concentrations, N_2 concentration has been fixed at the flow of 0.12 SCCM) has been grown on SCD IIa and SCD Ib substrates. Figure 1 presents the photographs of the B–N co-doped diamond grown on SCD IIa and SCD Ib substrates. (These photographs have been captured before the annealing process.) Figure 1 (a) shows the B/N co-doped diamond (B/C ∼ 2500 ppm) on SCD IIa, which appears as almost colorless. Whereas by increasing the B/C ∼ 5000 ppm (figure 1(b)), CVD diamond/SCD IIa appeared in light blue color. Further, B/C concentration increased to 7500 ppm, the CVD diamond/SCD IIa looks like a blue diamond (figure 1(c)). The blue color of CVD diamond layers is raised from the emission of boron vacancy (BV) color centers, which have been formed during the diamond growth in the CVD process. Figures 1 (d)–(f) represents the photographs of B/N doped diamond grown on SCD Ib substrates, here the color of CVD diamond layers has been seeming similar to the color of SCD Ib substrates. The color of B/N doped CVD diamond on both SCD IIa and SCD Ib substrates has not been altered by the annealing process.

AFM surface topography images of B/N co-doped diamond on HPHT-SCD substrates have been obtained over the area of 10 μm × 10 μm to investigate the roughness and surface morphology. AFM topography of the B/N co-doped CVD diamond on SCD IIa has been shown in figures 2 (a)–(c), for B/C ∼ 2500 ppm to B/C ∼ 7500 ppm, respectively with constant N_2 flow of 0.12 SCCM. The surface of the homoepitaxial CVD diamond layer on SCD IIa is flat and smoother for B/C ∼ 2500 ppm [figure 2(a)] with average surface roughness (Ra) ∼ 1.31 nm and root mean square roughness (Rq) ∼ 2.26 nm has been observed because of substrate's good surface condition and low boron doping levels. Further, hillocks with flat (FHs) and pyramidal (PHs) shapes were formed [figure 2(b)] for the B/C ∼ 5000 ppm, due to stacking faults or dislocations at interface between CVD layer and substrate, which were formed at the initial stage of growth by the presence of metal impurities [39–41]. In addition, the hillock structures are favorably produced on un-etchable and immobile defect sites, where the carbon atoms are more reactive than normal surface carbons, results in preferential growth of propagating the defect upwards [42]. However, enhancement of N-incorporation at hillock kind of structures has been observed and which shown the path way for identifying the hillock-localized NV center ensembles for quantum technology applications [43]. The spherical-shaped grains [unepitaxial crystals (UCs)] were observed on the CVD diamond surface, these are mainly due to the fact that their nucleation occurs at contaminants and the influence of growth plasma [39, 44]. Monte Carlo Simulations described that the UCs are formed by misoriented growth islands merging, where each island forming a grain [42]. The Ra and Rq values have been increased to 13.07 nm and 21.26 nm, respectively for the CVD diamond layer grown with B/C ∼ 5000 ppm on SCD IIa.

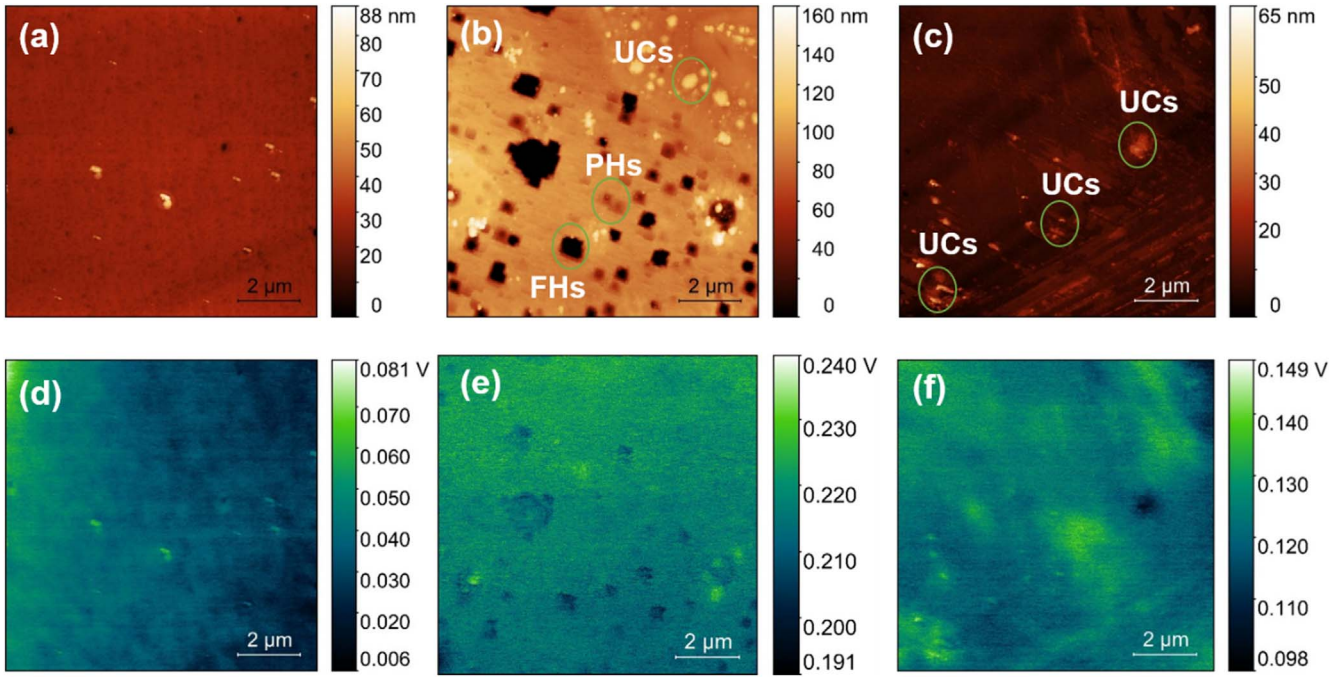

Figure 2. AFM topography of B/N co-doped CVD diamond on (with fixed N/C = 0.02) SCD IIa; (a) B/C ~ 2500 ppm (b) B/C ~ 5000 ppm (c) B/C ~ 7500 ppm, and KPFM CPD images of B/N co-doped CVD diamond (with fixed N/C = 0.02) on SCD IIa; (d) B/C ~ 2500 ppm (e) B/C ~ 5000 ppm (f) B/C ~ 7500 ppm.

Figure 2(C) exhibiting the surface topography of the CVD diamond layer grown on SCD IIa with B/C ~ 7500 ppm, revealing the Ra and Rq values of 1.86 nm and 2.92 nm, respectively. The surface of the CVD layer on SCD IIa consists of UCs in the form of islands and patches (figure 2(c)), which may be originating from the secondary nucleation from the precipitation of boron at a high B doping level [45]. Therefore, it confirms that B doping up to a minimal level does not create any surface features, but exceeding a certain level of B doping results in the formation of UCs even for the high-quality type IIa SCD substrates. However, the presence of metal impurities also can steer to the formation of FHs and PHs, which are the reason for the high surface roughness of CVD diamond/SCD IIa, grown at a B doping concentration of B/C ~ 5000 ppm. The SCD substrates were cleaned with acid mixtures and RCA process before loading to the substrate, therefore the presence of metal impurities on SCD substrates might be from the growth chamber or the growth plasma. The metal impurities might be the boron atoms, which did not participated in doping into diamond at initial growth due to the presence of oxygen in growth plasma [46].

Further, KPFM measurements of B/N co-doped CVD diamond/SCD IIa substrates have been illustrated in figures 2(d)–(f). The CPD values of 0.006–0.081 V for B/C ~ 2500 ppm (figure 2(e)), 0.191–0.240 V for B/C ~ 5000 ppm (figure 2(f)), and 0.098–0.149 V for B/C ~ 7500 ppm (figure 2(f)) have been observed for CVD diamond/SCD IIa samples. The low CPD values are attained for low B doping of B/C ~ 2500 ppm, and the CPD values have been increased with B doping of B/C ~ 5000 ppm. However, a further increase in B doping of B/C ~ 7500 ppm, results in a decrease in CPD values. Furthermore, the CPD values of each condition showing a distribution over the surface, which indicates that even the CVD diamond surface is smoother and not having any significant surface features like grains and twins, the B and N doping might be not uniform. The CVD diamond layer's work function (φ) has been calculated from the CPD value of each sample, and the obtained φ values are 4.93 eV, 4.47 eV, and 4.84 eV for B/C ~ 2500 ppm, 5000 ppm, and 7500 ppm, respectively. The resultant of CPD and φ values of CVD diamond/SCD IIa samples with different B doping suggesting that the increase of B doping can decrease the work function up to a certain level of B (saturation) doping and further B doping might cause the increase in φ of CVD diamond/SCD IIa.

To investigate the substrate's effect on the quality and related properties of CVD diamond on SCD substrates, SCD Ib substrates have been used to grow the B/N doped CVD diamond with B doping levels of B/C ~ 2500 ppm to 7500 ppm. Figures 3(a)–(c) shows the AFM surface topography images of B/N co-doped CVD diamond on SCD Ib substrates. Figure 3(a) exhibiting the surface topography of CVD diamond/SCD Ib with doping of B/C ~ 2500 ppm, which depicts the appearance of FHs, PHs, and UCs (UCs aligned in rows). The FHS and PHs are formed because of stacking faults or dislocations at the interface [39, 40, 44]. The UCs are grown in CVD diamond layer due to contaminants and mis-oriented growth islands merging [42]. Ra value ~2.41, nm and Rq ~ 4.84 nm values are attained for CVD diamond/SCD Ib grown with B/C ~ 2500 ppm, and corresponding KPFM image has shown as figure 3(d), which reveals the CPD values ~0.055 to 0.211 V. Further, FHs, PHs, and conical shaped UCs were observed for the B/C ~ 5000 ppm

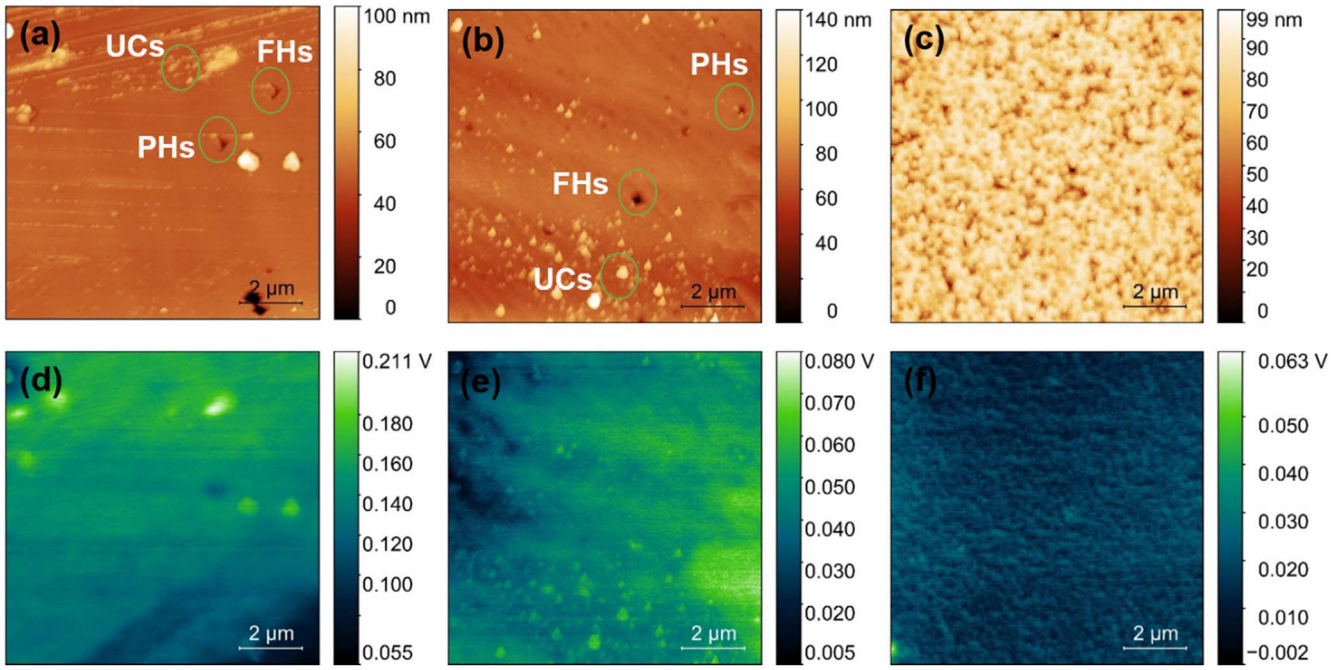

Figure 3. AFM topography of B/N co-doped CVD diamond layer (with fixed N/C = 0.02) on SCD Ib; (a) B/C ∼ 2500 ppm (b) B/C ∼ 5000 ppm (c) B/C ∼ 7500 ppm, and KPFM CPD images of B/N co-doped CVD diamond layer (with fixed N/C = 0.02) on SCD Ib; (d) B/C ∼ 2500 ppm (e) B/C ∼ 5000 ppm (f) B/C ∼ 7500 ppm.

(figure 3(b)), the origin of these defects is mainly due to stacking faults, dislocations at the interface, and boron aggregates (which are increasing with high B doping) [39, 40, 44, 46]. The surface roughness of CVD diamond/SCD Ib with B/C ∼ 5000 ppm has shown Ra and Rq values of 3.73 nm and 6.45 nm. Figure 3(e) depicts the CPD image of CVD diamond/SCD Ib with B/C ∼ 5000 ppm, which reveals the CPD values between 0.005 and 0.080 V. Figure 3(c) exhibiting the surface topography of CVD diamond/SCD Ib with B/C ∼ 7500 ppm, which is revealing rough surface with large aggregates with porous structure. These aggregates are connected but not appearing as a continuous film and are mainly UCs formed randomly with high density and Ra, Rq values of 7.60 nm and 9.52 nm are observed for this sample. The corresponding CPD image of the CVD diamond/SCD IIa is shown in figure 3(f), revealing the CPD distribution of −0.002 to +0.063 V.

Polarization micrographs were collected from CVD diamond layers grown on SCD IIa and SCD Ib substrates to find the origin FHs, PHs, and UCs due to presence of defects in diamond samples. Polarization microscopy is a widely used characterization technique to identify the defects, dislocations and strain in both the natural, HPHT and CVD-grown diamond by observing the birefringence patterns, which ensued due to changes in isotropic properties of diamond [47–49]. CVD diamond/SCD samples were rotated with respect to the cross-polarizers 0°, 45°, 90°, 135° and 180° to observe the birefringence from the defects in CVD diamond samples. Figure 4 displays the polarization micrographs (collected at the angle of 90°) of the CVD diamond/SCD IIa samples. Figures 4(a)–(c) showing the polarization microscopy images for before annealing of CVD diamond/SCD IIa for B/C ∼ 2500 ppm (figure 4(a)), B/C ∼ 5000 ppm (figure 4(b)), and B/C ∼ 7500 ppm (figure 4(c)). These images are depicting no sign of stacking faults or dislocations or strain-related birefringence patterns, however, FHs, PHs kind of defects were observed on the surface of CVD diamond/SCD IIa (figure 2(b)). The inability in attaining the birefringence patterns from stacking faults or dislocations caused by the formation of FHs/PHs might be due to the large measuring area of polarization microscopy and these defects are situated in few microns (The size of FHs or PHs ∼1–2 μm and measuring area ∼ hundreds of μm). Figures 4(d)–(f) exhibiting the polarization images for after annealing of CVD diamond/SCD IIa samples grown with B/C ∼ 2500 ppm, B/C ∼ 5000 ppm, and B/C ∼ 7500 ppm, respectively. The polarization micrographs of CVD diamond/SCD IIa have appeared similar to the as-grown samples (figures 4(a)–(c)), because of the high quality, lack of defects, and negligible strain in SCD IIa substrates. The FHs and PHs are only formed due to diamond growth plasma consisting of boron, which may have induced the formation of stacking faults and dislocations at the interface between SCD IIa substrate and the CVD diamond layer.

Figures 5(a)–(c) illustrating the polarization micrographs for before annealing of the CVD diamond/SCD Ib samples. The star-shaped birefringence pattern has been observed from the CVD diamond/SCD Ib sample grown with B/C ∼ 2500 ppm (figure 5(a)). The weak birefringence of this sample might be due to the strain in the SCD Ib substrate and not from the homoepitaxial layer. Furthermore, CVD diamond/SCD Ib samples grown using B/C ∼ 5000 ppm (figure 5(b)), and B/C ∼ 7500 ppm (figure 5(c)) have shown the strong cross-shaped birefringence pattern from the strain fields in the SCD Ib substrates. Figures 5(b) and (c) shown the regions

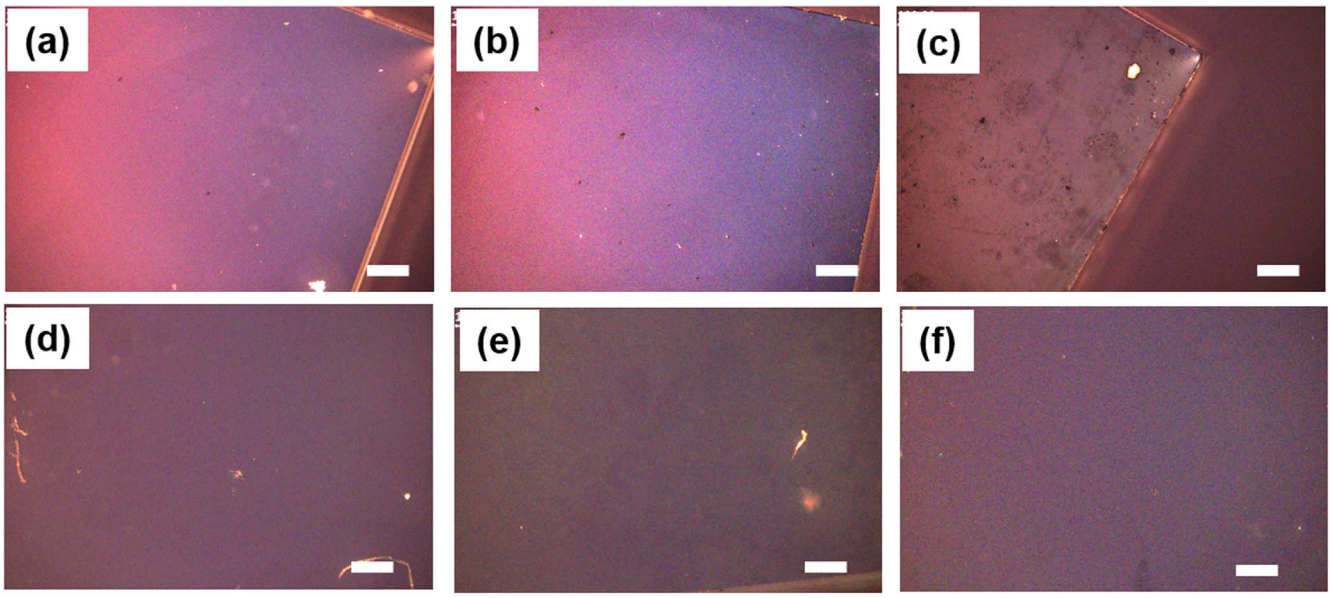

Figure 4. Polarization micrographs of B/N co-doped CVD diamond layer (with fixed N/C = 0.02) on SCD IIa; (a) B/C ∼ 2500 ppm, (b) B/C ∼ 5000 ppm, (c) B/C ∼ 7500 ppm showing for before annealing and (d) B/C ∼ 2500 ppm, (e) B/C ∼ 5000 ppm, (f) B/C ∼ 7500 ppm, showing for after annealing [scale bar ∼ 100 μm].

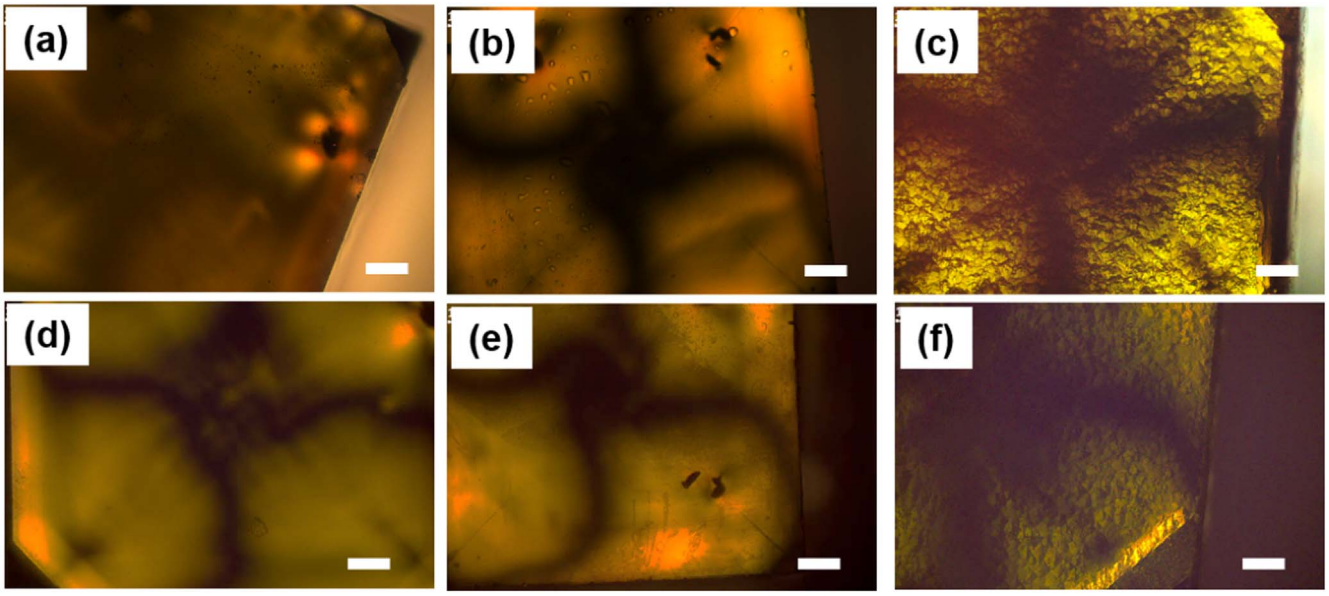

Figure 5. Polarization micrographs of B/N co-doped CVD diamond layer (with fixed N/C = 0.02) on SCD Ib; (a) B/C ∼ 2500 ppm, (b) B/C ∼ 5000 ppm, (c) B/C ∼ 7500 ppm showing for before annealing and (d) B/C ∼ 2500 ppm, (e) B/C ∼ 5000 ppm, (f) B/C ∼ 7500 ppm, showing for after annealing [scale bar ∼ 100 μm].

with four bright petals. This birefringence pattern was earlier observed by Pinto and Jones in the CVD-grown diamond as a result of dislocations bundles in the crystal [49]. Hoa *et al* in turn used experiments and a birefringence model to describe unit dislocation in the HPHT and MPACVD diamond [47]. Furthermore, polarization microscopy images are collected from the annealing performed CVD diamond/SCD Ib samples (figures 5(d)–(f)) to observe the influence of annealing on defects and related birefringence. Figure 5(d) shows the polarization micrograph of CVD diamond/SCD Ib grown with B/C ∼ 2500 ppm, which depicts the absence of star shaped birefringence and the cross-shaped birefringence that appeared after annealing. Figures 5(e)–(f) represents the polarization micrographs of CVD diamond/SCD Ib of B/C ∼ 5000 ppm and B/C ∼ 7500 ppm, respectively. The cross-shaped birefringence has been observed from both of these samples with high brightness after annealing. The annealing process leads to migration of partial dislocations and their merging into perfect dislocation, and vanishing of Shockley stacking faults [50].

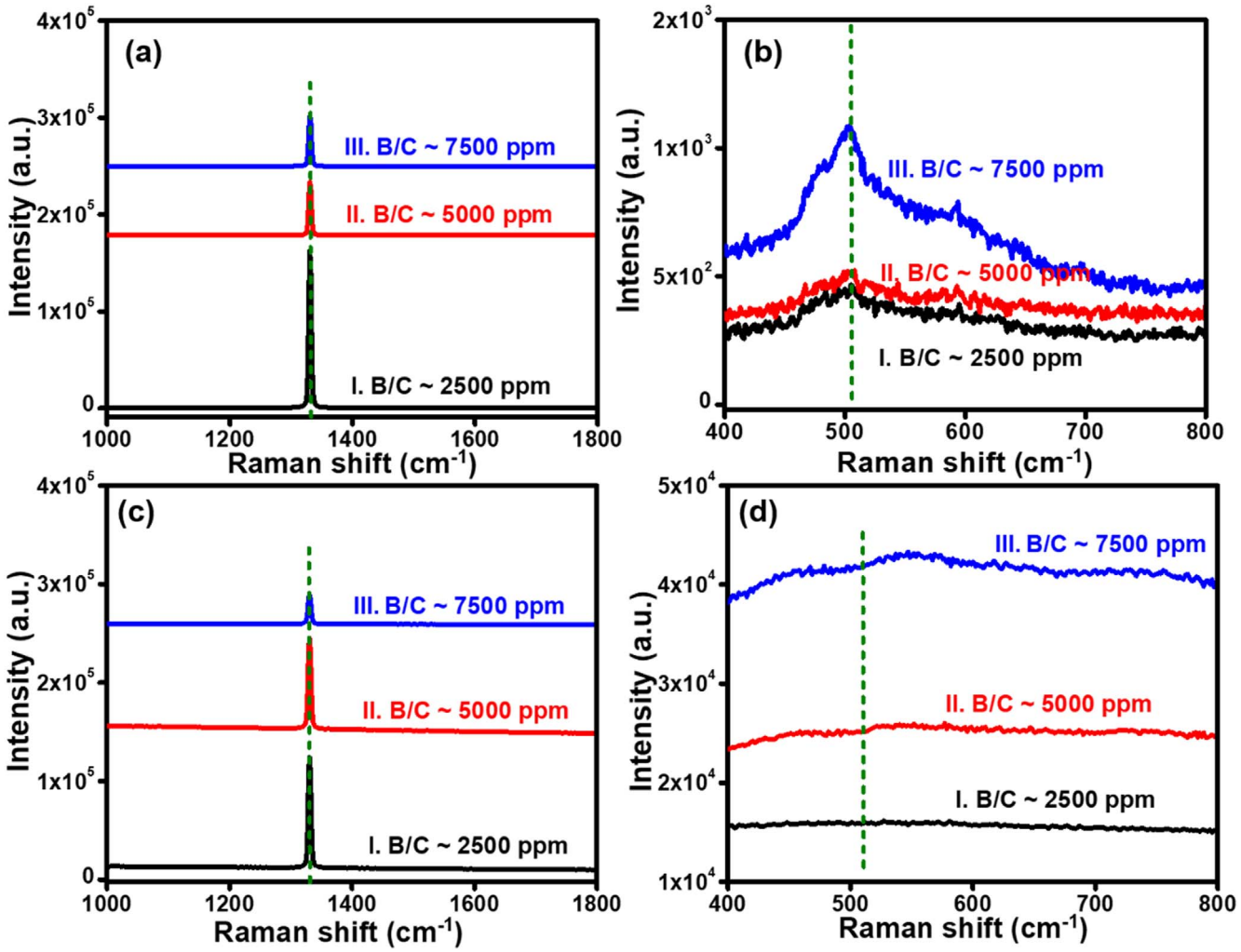

Figure 6. Raman spectra of (a) B/N co-doped CVD diamond layer (with fixed N/C = 0.02) on SCD IIa; (I) B/C ~ 2500 ppm (II) B/C ~ 5000 ppm (III) B/C ~ 7500 ppm, and (b) Raman spectra in the range of 400–800 cm^{-1} for identifying the response of B in CVD diamond; (I) B/C ~ 2500 ppm (II) B/C ~ 5000 ppm (III) B/C ~ 7500 ppm. Raman spectra of (c) B/N co-doped CVD diamond layer (with fixed N/C = 0.02) on SCD Ib; (I) B/C ~ 2500 ppm (II) B/C ~ 5000 ppm (III) B/C ~ 7500 ppm, and (d) Raman spectra in the range of 400–800 cm^{-1} for identifying the response of B in CVD diamond; (I) B/C ~ 2500 ppm (II) B/C ~ 5000 ppm (III) B/C ~ 7500 ppm.

Raman spectra have been collected from the as-grown CVD diamond on SCD IIa and SCD Ib substrates to investigate the carbon bonding characteristics and phases. Initially, Raman spectra of as-received SCD substrates have been collected (data not shown here) for reference. The characteristic first-order Raman line of diamond has been centered at 1331.41 cm^{-1} [full width half maximum (FWHM) ~ 4.38 cm^{-1}] for SCD IIa, and 1331.11 cm^{-1} (FWHM ~ 4.86 cm^{-1}) for SCD Ib substrates. However, a defect-free and high-quality diamond shows the first-order Raman line centered at 1332 cm^{-1} with FWHM value of 5–10 cm^{-1} [51]. The as-received SCD Ib samples revealing a characteristic band shift towards lower wavenumbers, i.e. blue shift, because the SCD Ib substrates consist of a high density of N ensembles, as a result, the blue shift is more prominent than the SCD IIa substrates. The presence of impurities and related stress causes the blue shift in as-received samples, however, the amount of impurities in SCD IIa are very low due to its high quality compared to SCD Ib.

Figures 6(a)–(d) shows the Raman spectra of CVD diamond/SCD samples. Figure 6(a) showing the Raman spectra of CVD diamond/SCD IIa samples, which illustrating the characteristic first-order Raman line centered at a unique Raman shift ~1330.65 cm^{-1} with different FWHM values for different B/C doping levels. The CVD diamond/SCD IIa samples demonstrated the FWHM values of 4.23 cm^{-1}, 4.19 cm^{-1}, and 4.22 cm^{-1} for B doping of B/C ~ 2500 ppm [curve I in figure 6(a)], B/C ~ 5000 ppm (curve II in figure 6(a)), and B/C ~ 7500 ppm (curve III in figure 6(a)), respectively. Similarly, Raman spectra of CVD diamond/SCD Ib samples (figure 6(c)) showing the first-order Raman line at 1330.65 cm^{-1} with different FWHM values, i.e. 4.43 cm^{-1}, 4.80 cm^{-1}, and 4.88 cm^{-1} for growth conditions of B/C ~ 2500 ppm (curve I. Figure 6(c)), B/C ~ 5000 ppm (curve II. Figure 6(c)), and B/C ~ 7500 ppm (curve III. Figure 6(c)), respectively. All these samples showed the high intense first-order Raman line, which indicates the existence of sp^3 hybridization and no other phases of carbon [52].

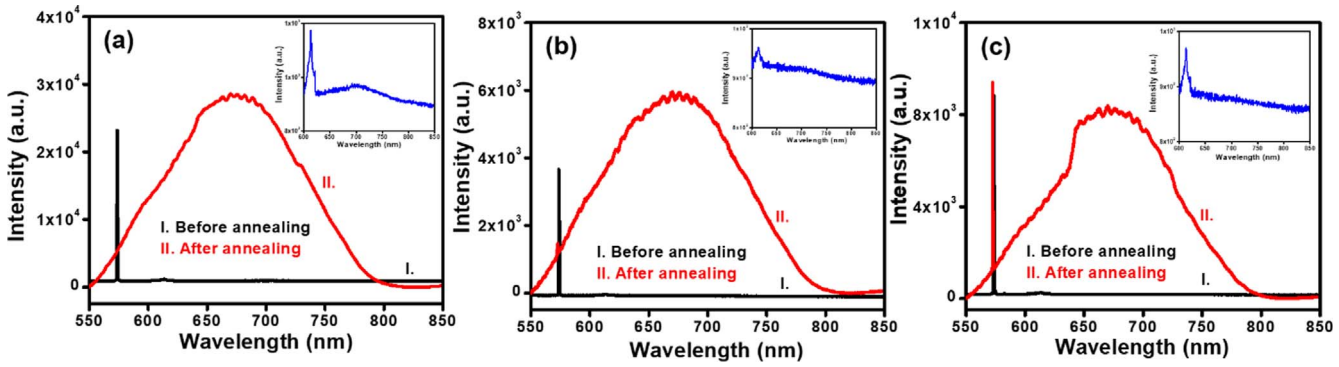

Figure 7. Photoluminescence spectra of B/N co-doped CVD diamond (with fixed N/C = 0.02) on SCD IIa; (a) B/C ∼ 2500 ppm: I. Before annealing, II. After annealing. (b) B/C ∼5000 ppm: I. Before annealing, II. After annealing. (c) B/C ∼ 7500 ppm: I. Before annealing, II. After annealing. Insets showing the enlarged PL spectra in the range of 600–850 nm.

Different B doping levels of CVD diamond layers on SCD IIa and SCD Ib have demonstrated a blueshift, even more, downshift compared to the as-received SCD substrates. Whereas, the narrowing of FWHM has been observed for CVD diamond compared to SCD substrates, which indicates the high quality of the homoepitaxial CVD diamond layer. However, it should be noted that the first-order Raman line of all these samples centered at 1330.65 cm^{-1} even with high B doping. The N doping into CVD diamond leads to the blueshift because of low atomic radius compared to carbon, while the B doping into CVD diamond results in redshift due to a high atomic radius, by the B/N co-doping these two kinds of shifts should be balanced [53]. Though in the present study the N flow has been kept constant, and B doping has been increased from B/C ∼ 2500 ppm to 7500 ppm, therefore one expects the number of B atoms doped into CVD diamond should be higher than N atoms. In this scenario, the predominant B doping should lead to the redshift, however, in the present study, high B doped samples exhibited the first-order Raman line at 1330.65 cm^{-1}, which is contradictory to the [53]. High B doped polycrystalline diamond films have shown the blueshift in our previous study [54], and characteristic upshift of first-order Raman line has been observed for N doped diamond films [55]. Therefore, the blueshift of the first-order Raman line due to B doping should be balanced by the redshift caused by N doping.

In addition, Raman spectra have been collected in a span of 200–800 cm^{-1} to investigate the B presence in the CVD diamond. Figure 6(b) showing the broad peaks around 500 cm^{-1} attributed to the presence of boron in CVD diamond/SCD IIa for boron doping of B/C ∼ 2500 ppm (curve I in figure 6(b)), B/C ∼ 5000 ppm (curve II in figure 6(b)), and B/C ∼ 7500 ppm (curve III in figure 6(a)), respectively [56]. Whereas, for low boron doping level of B/C ∼ 2500 ppm in CVD diamond/SCD samples, Raman response of the boron is less significant (curve I in figure 6(b)). Furthermore, Raman spectra of CVD diamond/SCD Ib samples shown in figure 6(d), which describing the response from the B for the samples grown with B/C ∼ 5000 ppm (curve II in figure 6(b)) and B/C ∼ 7000 ppm (curve III in figure 6(b)) demonstrating the vibration of boron in diamond [56]. However, the B response peaks are much wider due to the background luminescence of the SCD Ib substrates. In case the CVD diamond grown with B/C ∼ 2500 not shown the vibrations from B due to low doping levels and high background luminescence from substrate. Overall, the Raman spectra of CVD diamond on SCD IIa and SCD Ib samples are revealing the successful boron doping at average to high boron injection into growth plasma. The bi-axial stress in these SCD substrates has been calculated using the change in the Raman shift [57], and the stress values ∼0.3599 GPa and 0.5429 GPa are attained for SCD IIa and SCD Ib, respectively. Similarly, the stress value in the CVD diamond was also calculated as described in [57] and attained the stress value of 0.8235 GPa for all the samples. The attained stress value illustrating the strain in CVD diamond by B–N co-doping, which is higher than the as-received SCD substrates.

PL spectra of CVD diamond/SCD IIa samples haven collected before and after the annealing and shown in figures 7(a)–(c). Before annealing, a sharp emission line at 573.64 nm has been observed from all these samples, which are grown with B/C ∼ 2500 ppm (curve I in figure 7(a)), B/C ∼ 5000 ppm (curve I in figure 7(b)), and B/C ∼ 7500 ppm (curve I in figure 7(c)). The sharp emission line at 573.64 nm is attributed to the characteristic Raman line of the diamond [58]. Furthermore, a small hump was observed nearly around 600 nm, to perceive this emission clearly, enlarged PL spectra have been plotted in the range of 600–850 nm, and shown as insets in the figures 7(a)–(c). The enlarged PL spectra is revealing the emission at 613 nm, and 620 nm, which is generally observed for the untreated HPHT substrates [59], implying the emission is attributed to the substrate. In addition, PL spectra of the CVD diamond on SCD IIa demonstrating no sign of any emission of diamond color centers like NV centers, which are expected to be formed due to N doping.

CVD diamond/SCD samples were annealed at 800 °C for 2 h in a vacuum and subsequently cleaned with H_2SO_4 + HNO_3 mixture at 200 °C for 1h to remove the few layers of graphite, which were formed on the CVD diamond surface during the annealing process. PL spectra of annealed, cleaned CVD diamond/SCD IIa samples shown as curve II in figure 7(a) for B/C ∼2500 ppm, curve II in figure 7(b) for B/C ∼5000 ppm and curve II in figure 7(c) for B/C ∼ 7500 ppm. PL of these

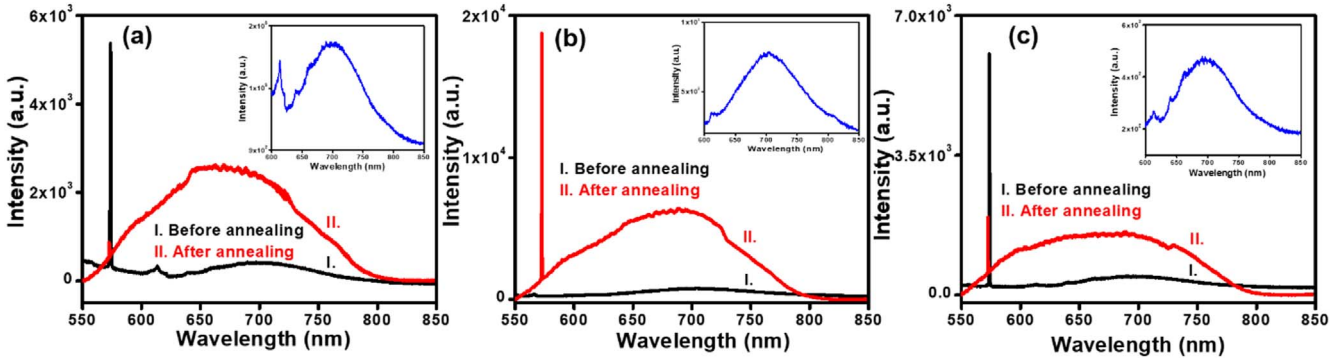

Figure 8. Photoluminescence spectra of B/N co-doped CVD diamond (with fixed N/C = 0.02) on SCD Ib; (a) B/C ∼ 2500 ppm: I. Before annealing, II. After annealing. (b) B/C ∼ 5000 ppm: I. Before annealing, II. After annealing. (c) B/C ∼ 7500 ppm: I. Before annealing, II. After annealing. Insets showing the enlarged PL spectra in the range of 600–850 nm.

samples clearly showing the typical NV spectra ranging from 550 to 800 nm [7, 8], however, zero phonon lines (ZPLs) of NV° and NV^{-} are not clearly visible due to strong phonon sidebands (PSBs). PL spectra of the annealed CVD diamond/SCD IIa samples confirming that the annealing process assists in the formation of NV centers. Thus, the NV centers have been created in the annealing process by the migration of vacancies in the vicinity of substitutional N atoms at a temperature of above 650 °C.

Figures 8(a)–(c) illustrating the PL spectra of CVD diamond/SCD Ib for before annealing for samples grown with B/C ∼ 2500 ppm (curve I in figure 8(a)), B/C ∼ 5000 ppm (curve I in figure 8(b)), and B/C ∼ 7500 ppm (curve I in figure 8(c)). A sharp emission line has been observed at 573.64 nm, which is related to the Raman vibration line [58]. Due to high intensity of Raman line, the typical NV emission has been not appeared clearly. Therefore, the enlarged PL spectra (600–850 nm) of CVD diamond/SCD Ib shown as inset in figure 8(a) for B/C ∼ 2500 ppm, inset in figure 8(b) for B/C ∼ 5000 ppm, and inset in figure 8(c) for B/C ∼ 7500 ppm. The enlarged PL spectra of all these samples have been demonstrating the emission line at 613 nm [59], a ZPL at 638 nm and wide PSBs from typical NV^{-} emission [7]. NV emission spectra have been observed only from the as-grown CVD diamond on SCD Ib substrates rather not from the CVD diamond on SCD IIa, even with unique growing conditions. NV emission of as-grown CVD diamond/SCD Ib substrates might be from the SCD Ib substrates because SCD Ib substrates are containing the intrinsic N impurities, the NV centers might be created in SCD Ib substrates while CVD diamond growth at 900 °C. However, CVD diamond/SCD Ib grown with B/C ∼ 5000 ppm sample exhibiting quite different PL emission spectra by emission at 883 nm (spectrum not shown) are attributed ZPLs of Ni related emission [60]. The emission of Ni impurities is from the SCD Ib substrates, which are doped in the HPHT synthesis process. PL spectra of annealed CVD diamond/SCD Ib samples shown curve II in figure 8(a) for B/C ∼ 2500 ppm, curve II in figure 8(b) for B/C ∼ 5000 ppm, and curve II in figure 8(c) for B/C ∼ 7500 ppm. PL spectra these annealed samples exhibiting the characteristic NV emission with PSBs [curve II in figures 8(a)–(c)], similar to those as-grown CVD Diamond/SCD Ib samples. In addition, a strong emission line at 572.5 nm, which is related to the Raman line of diamond [58]. In the case of Ni-related emissions from CVD diamond/SCD Ib grown with B/C ∼ 5000 ppm was vanished after the annealing process (PL spectrum not shown).

XPS spectra were collected to investigate the successful doping of B and N atoms into the CVD diamond/SCD IIa samples grown with low B doping (B/C ∼ 2500 ppm) and high B doping (B/C ∼ 7500 ppm) concentrations. The C 1s core line of CVD diamond/SCD IIa samples growing with B/C ∼ 2500 ppm and 7500 ppm have shown binding energy of 285 eV. Figure 9(a) depicts the C 1s core line of CVD diamond grown with B/C ∼ 2500 ppm, it is further deconvoluted into five Lorentzian peaks such as peak at 284.84 eV for C–C bonding of C–sp^3 carbon (59.67 %), peak at 284.12 eV for C=C bonding of C–sp^2 carbon (6.84 %), while peak at 285.61 eV for C–N bonding of N–sp^3 carbon (18.65 %), peak at 287.36 eV for N=sp^2 carbon (5.83 %), and a small peak at 283.07 eV for B–sp^3 carbon (1.01 %) [61–64].

The C 1s core line of CVD diamond grown with high boron doping of B/C ∼ 7500 ppm has been shown as figure 9(b). The C 1s line further deconvoluted into five peaks, which are depicted at 284.88 eV for C–C of C–sp^3 carbon (29.34%), peak at 284.18 eV for C=C of C–sp^2 carbon (44.85%), whereas other peaks at 285.7 eV for C–N bonding of N–sp^3 carbon (10.71%), at 287.36 eV for N=sp^2 carbon (4.55%) and peak at 282.95 eV for B–sp^3 carbon (2.21%) [61–64]. XPS spectra confirming that low and high levels of boron with constant nitrogen addition into growth plasma lead to the effective addition of boron into CVD diamond layers prepared on SCD substrates. High B doping of CVD diamond demonstrating an increase in C–sp^2 carbon (6.84%–44.85%) and B–sp^3 carbon (1.01%–2.21%), which indicates the increase in B doping level into CVD diamond resulting in enhancing the B doping concentration and decrease in diamond quality (enhancing the non-diamond phase). Furthermore, an increase in B doping also influencing the N doping efficiency by decreasing the N–sp^3 carbon (18.65%–10.71%) and N=sp^2 carbon (8.53%–4.55%).

Figure 9(c) illustrating the three deconvoluted B 1s peaks at binding energies of 185.7 eV for B–sp^3 boron, 188.2 eV for B–sp^3 carbon, and 191 eV for B–sp^3 oxygen for CVD

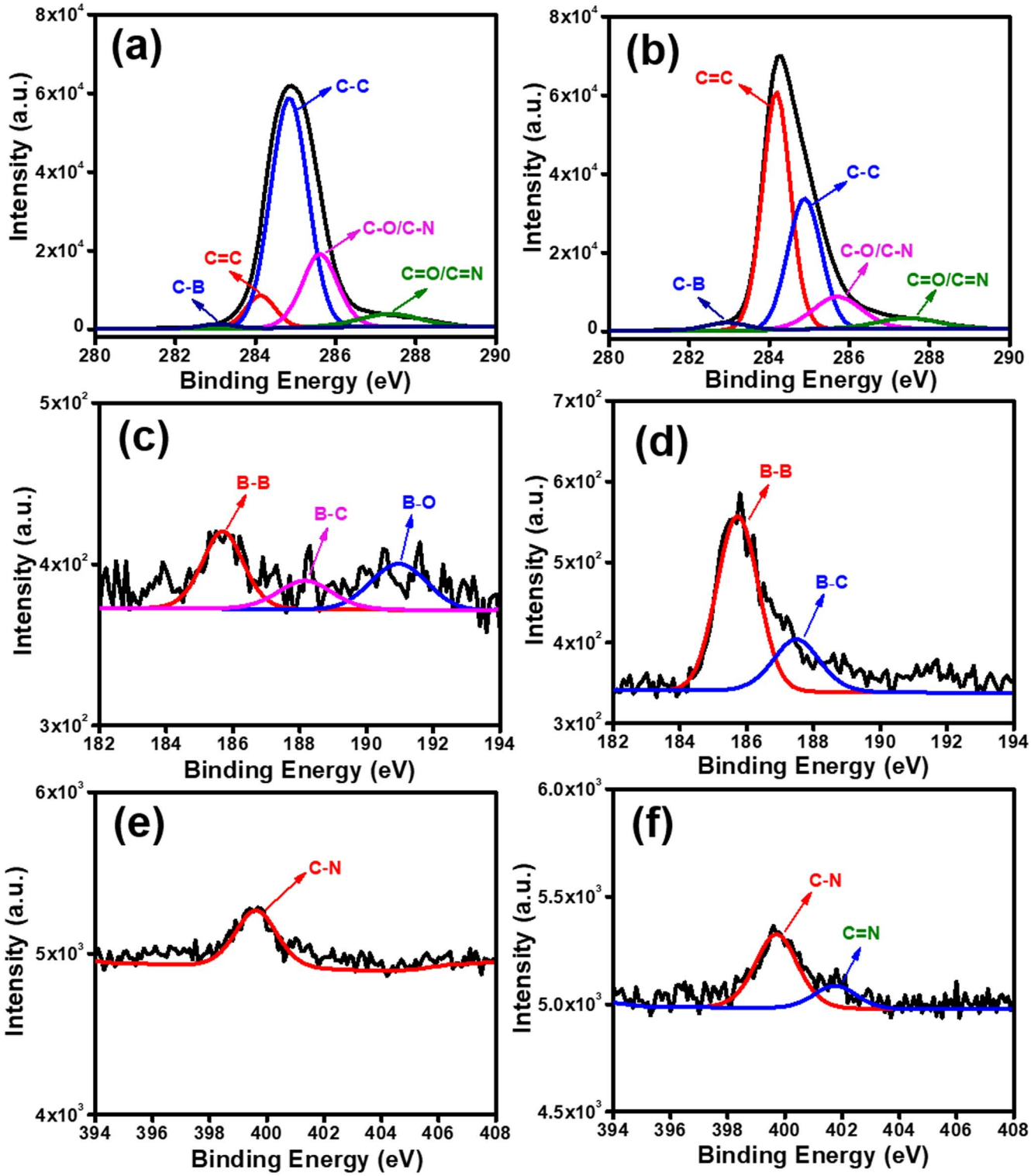

Figure 9. XPS fitted curves of B/N co-doped CVD diamond/SCD IIa with boron doping level of B/C ∼ 2500 ppm; (a) C 1s spectra (c) B 1s spectra (e) N 1s spectra; XPS fitted curves of B/N co-doped CVD diamond/SCD IIa with boron doping level of B/C ∼ 7500 ppm; (b) C 1s spectra (d) B 1s spectra (f) N 1s spectra.

diamond grown with boron doping of B/C ∼ 2500 ppm [65]. Furthermore, the CVD diamond prepared by B/C ∼ 7500 ppm showing the deconvoluted B 1s peaks at 185.7 eV for B–sp^3 boron and 187.5 eV for B–sp^3 carbon (figure 9(d)), which indicates that the doped B atoms form a bond with carbon atoms and also the creation of the B dimers [65, 66]. B 1s peak intensities of B–B and B–C are increased with boron doping concentration. Figure 9(e) shows the XPS spectra of CVD diamond/SCD IIa grown with B/C ∼ 2500 ppm, describing the deconvoluted N 1s peak at a binding energy of 399.6 eV for N–sp^3 carbon [10, 25]. Whereas, boron doping levels of B/C ∼ 7500 ppm (figure 9(f)), N 1s peak

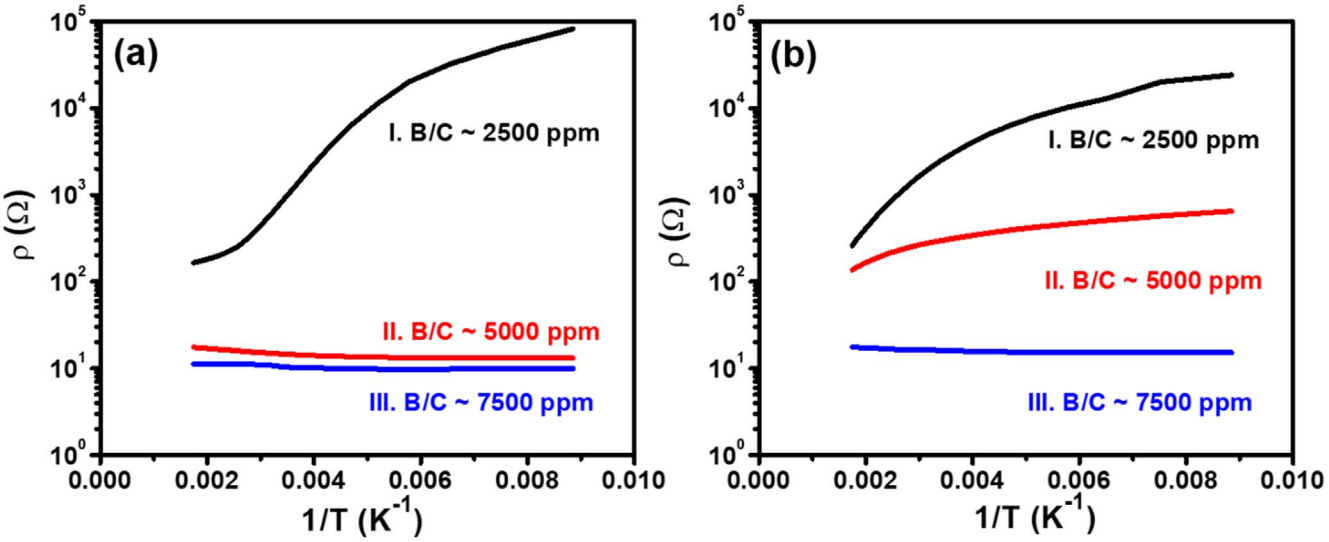

Figure 10. Temperature versus resistance measurements of (a) B/N co-doped CVD diamond/SCD IIa with boron doping of I. B/C ~ 2500 ppm, II. B/C ~ 5000 ppm, III. B/C ~ 7500 ppm. (b) B/N co-doped CVD diamond/SCD Ib with boron doping of I. B/C ~ 2500 ppm, II. B/C ~ 5000 ppm, III. B/C ~ 7500 ppm.

deconvoluted into two peaks at binding energies of 399.7 eV for N–sp^3 carbon and 401.8 eV for N–sp^2 carbon [10, 25], which describes the inclusion of N atoms into CVD diamond and bonding with carbon atoms. Though, the increase in boron doping results in the formation of the C=N phase.

The CVD diamond/SCD IIa samples revealed the characteristic electrical resistance values (at room temperature) of 680.76 Ω for B/C ~ 2500 ppm, 14.64 Ω for B/C ~ 5000 ppm, and 9.30 Ω for B/C ~ 7500 ppm at room temperature. CVD diamond/SCD Ib samples shown the electrical resistance of 2300.40 Ω for B/C ~ 2500 ppm, 345.70 Ω for B/C ~ 5000 ppm, and 16.55 Ω for B/C ~ 7500 ppm at room temperature. Furthermore, electrical properties of CVD diamond films grown on SCD IIa and SCD Ib substrates have been measured at temperatures ranging from 83.15 to 573.15 K. The measured resistance values at different temperatures were plotted as resistance versus reciprocal temperature (R versus $1/T$), and shown in figures 10(a) and (b) for CVD diamond grown on SCD IIa and SCD Ib substrates, respectively. The activation energy (E_a) of the B in CVD diamond films was obtained by the Arrhenius law using the equation: $E_a = R \times$ slope of [R versus $1/T$], $R \sim$ Rydberg constant [66, 67]. E_a values of CVD diamond/SCD IIa samples have demonstrating $E_a \sim 3788.59$ J mol^{-1} (39.3 meV) for CVD diamond grown with B/C ~ 2500 ppm, $E_a \sim$ the deconvoluted B 1s peaks at 185.7−171.38 J mol^{-1} (−1.8 meV) for B/C ~ 5000 ppm, $E_a \sim -92.81$ J mol^{-1} (−1.0 meV) for B/C ~ 7500 ppm. In addition, CVD diamond/SCD Ib samples revealing the E_a values of 2490.32 J mol^{-1} (25.8 meV), 809.86 J mol^{-1} (8.4 meV), and −10.66 J mol^{-1} (−0.1 meV) for CVD diamond synthesized with B/C ~ 2500 ppm, B/C ~ 5000 ppm, and B/C ~ 7500 ppm, respectively.

The E_a value ~930 meV has been obtained for undoped polycrystalline diamond films [68]. Whereas, lightly doped BDD films shown the characteristic E_a value is around 38 meV, which is nearly close to the E_a values for low B doping of B/C 2500 ppm in this study [69, 70]. The R and E_a values of CVD diamond films have decreased with an increase in B/C up to 5000 ppm. These results, suggesting the efficient B incorporation into the diamond lattice. The addition of small amounts of N has an impact on enhancing the electrical conductivity [71], the present study, the addition of such low N flow might be beneficial for achieving lower resistance values for samples doping with B/C ~ 5000 ppm and 7500 ppm. However, the decrease in R-value is less significant for samples grown with B/C ~ 7500 ppm, compared to B/C ~ 5000 ppm, due to all the doped B atoms are not act as acceptors and formed the complexes with other atoms [21, 72]. In addition, the substrates have a prominent effect on R values for CVD diamond films grown on SCD IIa substrates demonstrated low R and E_a values.

4. Conclusions

To summarize, we have compared B/N co-doped diamond layers on SCD IIa and SCD Ib substrates grown by MPACVD. Tuning of boron doping concentration has shown a significant influence on plasma chemistry and layer composition. High-quality blue diamond was achieved at SCD IIa substrates at high B doping levels, whereas similar B doping concentration resulted in degenerated light green color at SCD Ib substrates. A smooth surface with a roughness of 2.26 nm was attained for low B doping, whereas hillock-like structures and unepitaxial diamond crystals have been grown for high boron doping levels pronounced at SCD surfaces. The *in-situ* co-doping induces synergistically crystal defects, which are even pronounced at average boron levels. Higher B concentrations impacted the increase of N incorporation into diamond layers revealed by XPS analysis. The increase of B/N co-doping ratios was also responsible for the reduction of nitrogen precipitation in CVD diamond promoting the

formation of increased density of NV centers displayed in PL spectra. Nevertheless, an efficient NV emission was achieved after thermal treatment of samples attributed to the migration vacancies to form the NV centers. Doping by boron decreases the work function down to 4.47 eV saturation level followed by its increase for larger doping levels attributed to the growth of sp2 degenerated diamond and formation of boron-clusters, which influences the NV emission due to quenching. The boron doping introduces impurities band revealed surficial conductivity in the range of a few Ohms, which is enhanced additionally by nitrogen co-doping particularly benefiting at low boron-doping. The tailoring of B/N co-doping CVD diamond at SCD substrates allowed to achieve high quality and low resistivity layers attractive in the frame of joint quantum/electronic or electrochemical applications. Moreover, the inhomogeneous hillock defects distribution could be utilized for specific coherence effects of NV centers for quantum sensing applications.

Acknowledgments

The authors would like to thank the Polish Science grant TEAM NET POIR.04.04.00-00-1644/18 for funding.

Data availability statement

The data generated and/or analysed during the current study are not publicly available for legal/ethical reasons but are available from the corresponding author on reasonable request.

Authorship contribution statement

Srinivasu Kunuku: Conceptualization, Visualization, Investigation, Validation, Writing—original draft. **Mateusz Ficek:** Conceptualization, Methodology, Visualization, Writing—original draft. **Aleksandra Wieloszynska:** Polarization microscopy measurements. **Magdalena Tamulewicz–Szwajkowska:** AFM and KFM measurements, analysis. **Krzysztof Gajewski:** Investigation. **Miroslaw Sawczak:** Raman spectroscopy measurements and analysis. **Aneta Lewkowicz:** Photoluminescence measurements and analysis. **Jacek Ryl**: XPS measurements and analysis. **Tedor Gotszalk:** Formal analysis, Supervision. **Robert Bogdanowicz:** Writing—review and editing, Funding acquisition, Supervision.

Declaration of competing interest

The authors declare that they have no competing interests.

ORCID iDs

Srinivasu Kunuku https://orcid.org/0000-0002-0648-1226
Mateusz Ficek https://orcid.org/0000-0003-2334-9697
Magdalena Tamulewicz-Szwajkowska https://orcid.org/0000-0002-7382-011X
Krzysztof Gajewski https://orcid.org/0000-0001-6218-0658
Jacek Ryl https://orcid.org/0000-0002-0247-3851
Tedor Gotszalk https://orcid.org/0000-0003-4182-9192
Robert Bogdanowicz https://orcid.org/0000-0002-7543-2620

References

[1] Gruen D M 1999 Nanocrystalline diamond films *Annu. Rev. Mater. Sci.* **29** 211–59
[2] Angus J C and Low-Pressure H C C 1988 Metastable growth of diamond and 'diamondlike' phases *Science* **241** 913–21
[3] Nebel C E, Rezek B, Shin D, Uetsuka H and Yang N 2007 Diamond for bio-sensor applications *J. Phys. D: Appl. Phys.* **40** 6443–66
[4] Bar-Yam Y and Moustakas T D 1989 Defect-induced stabilization of diamond films *Nature* **342** 786–7
[5] Kalish R 1999 Doping of diamond *Carbon* **37** 781–5
[6] Lu H-C, Peng Y-C, Lin M-Y, Chou S-L, Lo J-I and Cheng B-M 2017 Analysis of boron in diamond with UV photoluminescence *Carbon* **111** 835–8
[7] Pezzagna S, Rogalla D, Wildanger D, Meijer J and Zaitsev A 2011 Creation and nature of optical centres in diamond for single-photon emission—overview and critical remarks *New J. Phys.* **13** 035024
[8] Orwa J O, Greentree A D, Aharonovich I, Alves A D C, Van Donkelaar J, Stacey A and Prawer S 2010 Fabrication of single optical centres in diamond—a review *J. Lumin.* **130** 1646–54
[9] Acosta V M *et al* 2009 Diamonds with a high density of nitrogen-vacancy centers for magnetometry applications *Phys. Rev.* B **80** 115202
[10] Schirhagl R, Chang K, Loretz M and Degen C L 2014 Nitrogen-vacancy centers in diamond: nanoscale sensors for physics and biology *Annu. Rev. Phys. Chem.* **65** 83–105
[11] Kraft A 2007 Doped diamond: a compact review on a new, versatile electrode material *Int. J. Electrochem. Sci.* **2** 355–85
[12] Yang N, Uetsuka H, Osawa E and Nebel C E 2008 Vertically aligned diamond nanowires for DNA sensing *Angew. Chem.* **120** 5261–3
[13] Ryl J, Burczyk L, Zielinski A, Ficek M, Franczak A, Bogdanowicz R and Darowicki K 2019 Heterogeneous oxidation of highly boron-doped diamond electrodes and its influence on the surface distribution of electrochemical activity *Electrochim. Acta* **297** 1018–27
[14] Sobaszek M, Siuzdak K, Ryl J, Bogdanowicz R and Swain G M 2020 The electrochemical determination of isatin at nanocrystalline boron-doped diamond electrodes: stress monitoring of animals *Sensors Actuators* B **306** 127592
[15] Sankaran K J *et al* 2018 Self-organized multi-layered graphene–boron-doped diamond hybrid nanowalls for high-performance electron emission devices *Nanoscale* **10** 1345–55
[16] Nidheesh P V, Divyapriya G, Oturan N, Trellu C and Oturan M A 2019 Environmental applications of boron-doped diamond electrodes: I. Applications in water and wastewater treatment *ChemElectroChem* **6** 2124–42
[17] Banerjee D *et al* 2020 Single-step grown boron doped nanocrystalline diamond-carbon nanograss hybrid as an efficient supercapacitor electrode *Nanoscale* **12** 10117–26

[18] Wang J, He Z, Tan X, Wang T, He X, Zhang L, Huang J, Chen G and Du K 2020 Hybrid supercapacitors from porous boron-doped diamond with water-soluble redox electrolyte *Surf. Coat. Technol.* **398** 126103

[19] Teukam Z *et al* 2003 Shallow donors with high n-type electrical conductivity in homoepitaxial deuterated boron-doped diamond layers *Nat. Mater.* **2** 482–6

[20] Werner M *et al* 1994 Charge transport in heavily B-doped polycrystalline diamond films *Appl. Phys. Lett.* **64** 595–7

[21] Gabrysch M, Majdi S, Hallén A, Linnarsson M, Schöner A, Twitchen D and Isberg J 2008 Compensation in boron-doped CVD diamond *Phys. Status Solidi* a **205** 2190–4

[22] Fan L *et al* 2021 Laser vibrational excitation of radicals to prevent crystallinity degradation caused by boron doping in diamond *Sci. Adv.* **7** eabc7547

[23] May P W, Ludlow W J, Hannaway M, Heard P J, Smith J A and Rosser K N 2008 Raman and conductivity studies of boron-doped microcrystalline diamond, facetted nanocrystalline diamond and cauliflower diamond films *Diam. Relat. Mater.* **17** 105–17

[24] Fang C, Jia X, Chen N, Li Y, Guo L, Chen L, Ma H and Liu X 2016 HPHT synthesis of N–H co-doped diamond single crystals *J. Cryst. Growth* **436** 34–9

[25] Zhang H, Li S, Li G, Su T, Hu M, Ma H, Jia X and Li Y 2017 Effect of B-S co-doping on large diamonds synthesis under high pressure and high temperature *Int. J. Refractory Met. Hard Mater.* **66** 26–30

[26] Li Y, Jia X, Ma H, Zhang J, Wang F, Chen N and Feng Y 2014 Electrical properties of diamond single crystals co-doped with hydrogen and boron *CrystEngComm* **16** 7547

[27] Li R 2005 A molecular dynamics study of boron and nitrogen in diamond *Solid State Commun.* **135** 155–7

[28] Hu M, Bi N, Li S, Su T, Hu Q, Ma H and Jia X 2017 Synthesis and characterization of boron and nitrogen co-doped diamond crystals under high pressure and high temperature conditions *CrystEngComm* **19** 4571–5

[29] Miao X, Chen L, Ma H, Fang C, Guo L, Fang S, Wang Y and Jia X 2018 Studies on HPHT synthesis and N defects of N-rich B-doped diamonds *CrystEngComm* **20** 7109–13

[30] Karna S and Vohra Y 2013 Effect of nitrogen on the growth of boron doped single crystal diamond *JMSR* **3** p43

[31] Issaoui R, Tallaire A, Mrad A, William L, Bénédic F, Pinault-Thaury M-A and Achard J 2019 Defect and threading dislocations in single crystal diamond: a focus on boron and nitrogen codoping *Phys. Status Solidi* a **216** 1900581

[32] Guo T *et al* 2021 Electrochemistry of nitrogen and boron Bi-element incorporated diamond films *Carbon* **178** 19–25

[33] Yang N, Yu S, Macpherson J V, Einaga Y, Zhao H, Zhao G, Swain G M and Jiang X 2019 Conductive diamond: synthesis, properties, and electrochemical applications *Chem. Soc. Rev.* **48** 157–204

[34] Li J, Wang Q, Liu Y, Jiang Z, Liu J, Li H and Yuan X 2021 Boron/nitrogen co-doped diamond electrode for highly efficient electrochemistry detection of aniline *Funct. Diam.* **1** 135–42

[35] Achard J, Jacques V and Tallaire A 2020 Chemical vapour deposition diamond single crystals with nitrogen-vacancy centres: a review of material synthesis and technology for quantum sensing applications *J. Phys. D: Appl. Phys.* **53** 313001

[36] Lühmann T, Meijer J and Pezzagna S 2021 Charge-assisted engineering of color centers in diamond *Phys. Status Solidi* a **218** 2000614

[37] Groot-Berning K *et al* 2014 Passive charge state control of nitrogen-vacancy centres in diamond using phosphorous and boron doping: passive charge state control of nitrogen-vacancy centres in diamond *Phys. Status Solidi* a **211** 2268–73

[38] Yap C M, Ansari K, Xiao S, Yee S Y, Chukka R and Misra D S 2018 Properties of near-colourless lightly boron doped CVD diamond *Diam. Relat. Mater.* **88** 118–22

[39] Tallaire A, Kasu M, Ueda K and Makimoto T 2008 Origin of growth defects in CVD diamond epitaxial films *Diam. Relat. Mater.* **17** 60–5

[40] Friel I, Clewes S L, Dhillon H K, Perkins N, Twitchen D J and Scarsbrook G A 2009 Control of surface and bulk crystalline quality in single crystal diamond grown by chemical vapour deposition *Diam. Relat. Mater.* **18** 808–15

[41] Ashkinazi E, Khmelnitskii R, Sedov V, Khomich A, Khomich A and Ralchenko V 2017 Morphology of diamond layers grown on different facets of single crystal diamond substrates by a microwave plasma CVD in CH_4-H_2-N_2 Gas Mixtures *Crystals* **7** 166

[42] Rodgers W J, May P W, Allan N L and Harvey J N 2015 Three-dimensional kinetic Monte Carlo simulations of diamond chemical vapor deposition *J. Chem. Phys.* **142** 214707

[43] Meynell S A, McLellan C A, Hughes L B, Mates T E, Mukherjee K and Jayich A C B 2020 Engineering quantum-coherent defects: the role of substrate miscut in chemical vapor deposition diamond growth *Appl. Phys. Lett.* **117** 194001

[44] Sawada H, Ichinose H, Watanabe H, Takeuchi D and Okushi H 2001 Cross-sectional TEM study of unepitaxial crystallites in a homoepitaxial diamond film *Diam. Relat. Mater.* **10** 2030–4

[45] Wang W L, Polo M C, Sánchez G, Cifre J and Esteve J 1996 Internal stress and strain in heavily boron-doped diamond films grown by microwave plasma and hot filament chemical vapor deposition *J. Appl. Phys.* **80** 1846–50

[46] Tsigkourakos M, Hantschel T, Xu Z, Douhard B, Meersschaut J, Zou Y, Larsson K, Boman M and Vandervorst W 2015 Suppression of boron incorporation at the early growth phases of boron-doped diamond thin films: Early growth phases of boron-doped diamond thin films *Phys. Status Solidi* a **212** 2595–9

[47] Hoa L T M, Ouisse T, Chaussende D, Naamoun M, Tallaire A and Achard J 2014 Birefringence microscopy of unit dislocations in diamond *Cryst. Growth Des.* **14** 5761–6

[48] Howell D 2012 Strain-induced birefringence in natural diamond: a review *EJM* **24** 575–85

[49] Pinto H and Jones R 2009 Theory of the birefringence due to dislocations in single crystal CVD diamond *J. Phys.: Condens. Matter* **21** 364220

[50] Masuya S, Hanada K, Oshima T, Sumiya H and Kasu M 2017 Formation of stacking fault and dislocation behavior during the high-temperature annealing of single-crystal HPHT diamond *Diam. Relat. Mater.* **75** 155–60

[51] Prawer S and Nemanich R J 2004 Raman spectroscopy of diamond and doped diamond *Phil. Trans. R. Soc.* A **362** 2537–65

[52] Elsherif O S, Vernon-Parry K D, Evans-Freeman J H and May P W 2012 Effect of doping on electronic states in B-doped polycrystalline CVD diamond films *Semicond. Sci. Technol.* **27** 065019

[53] Hu M, Bi N, Li S, Su T, Hu Q, Ma H and Jia X 2017 Synthesis and characterization of boron and nitrogen co-doped diamond crystals under high pressure and high temperature conditions *CrystEngComm* **19** 4571–5

[54] Rycewicz M, Ficek M, Gajewski K, Kunuku S, Karczewski J, Gotszalk T, Wlasny I, Wysmołek A and Bogdanowicz R 2021 Low-strain sensor based on the flexible boron-doped diamond-polymer structures *Carbon* **173** 832–41

[55] Bergman L and Nemanich R J 1995 Raman and photoluminescence analysis of stress state and impurity distribution in diamond thin films *J. Appl. Phys.* **78** 6709–19

[56] Mortet V, Vlčková Živcová Z, Taylor A, Frank O, Hubík P, Trémouilles D, Jomard F, Barjon J and Kavan L 2017 Insight into boron-doped diamond Raman spectra characteristic features *Carbon* **115** 279–84
[57] Ager J W and Drory M D 1993 Quantitative measurement of residual biaxial stress by Raman spectroscopy in diamond grown on a Ti alloy by chemical vapor deposition *Phys. Rev. B* **48** 2601–7
[58] Kurtsiefer C, Mayer S, Zarda P and Weinfurter H 2000 Stable solid-state source of single photons *Phys. Rev. Lett.* **85** 4
[59] Smith C P, Bosshart G, Ponahlo J, Hammer V M F, Klapper H and Schmetzer K 2000 Ge pol diamonds: before and after *Gems Gemol.* **36** 192–215
[60] Shames A I, Dalis A, Greentree A D, Gibson B C, Abe H, Ohshima T, Shenderova O, Zaitsev A and Reineck P 2020 Near-infrared fluorescence from silicon- and nickel-based color centers in high-pressure high-temperature diamond micro- and nanoparticles *Adv. Opt. Mater.* **8** 2001047
[61] Kusunoki I, Sakai M, Igari Y, Ishidzuka S, Takami T, Takaoka T, Nishitani-Gamo M and Ando T 2001 XPS study of nitridation of diamond and graphite with a nitrogen ion beam *Surf. Sci.* **492** 315–28
[62] Shirafuji J, Sakamoto Y, Furukawa A, Shigeta H and Sugino T 1995 X-ray photoelectron spectroscopy analysis of plasma-treated surfaces of diamond films *Diam. Relat. Mater.* **4** 984–8
[63] Ghodbane S, Ballutaud D, Omnès F and Agnès C 2010 Comparison of the XPS spectra from homoepitaxial {111}, {100} and polycrystalline boron-doped diamond films *Diam. Relat. Mater.* **19** 630–6
[64] Li J J, Zheng W T, Wu H H, Sun L, Gu G G, Bian H J, Lu X Y and Jin Z S 2003 Compositional and structural modifications of amorphous carbon nitride films induced by thermal annealing *J. Phys. D: Appl. Phys.* **36** 2001–5
[65] Liu X, Jia X, Zhang Z, Zhao M, Guo W, Huang G and Ma H 2011 Synthesis and characterization of new 'bcn' diamond under high pressure and high temperature conditions *Cryst. Growth Des.* **11** 1006–14
[66] Lagrange J-P, Deneuville A and Gheeraert E 1998 Activation energy in low compensated homoepitaxial boron-doped diamond films *Diam. Relat. Mater.* **7** 1390–3
[67] Mortet V *et al* 2021 Properties of boron-doped (113) oriented homoepitaxial diamond layers *Diam. Relat. Mater.* **111** 108223
[68] Muto Y, Sugino T, Shirafuji J and Kobashi K 1991 Electrical conduction in undoped diamond films prepared by chemical vapor deposition *Appl. Phys. Lett.* **59** 843–5
[69] Masood A, Aslam M, Tamor M A and Potter T J 1992 Synthesis and electrical characterization of boron-doped thin diamond films *Appl. Phys. Lett.* **61** 1832–4
[70] Collins A T and Williams A W S 1971 The nature of the acceptor centre in semiconducting diamond *J. Phys. C: Solid State Phys.* **4** 1789–800
[71] Sonoda S, Won J H, Yagi H, Hatta A, Ito T and Hiraki A 1997 Effect of nitrogen incorporation on electrical properties of boron-doped diamond films *Appl. Phys. Lett.* **70** 2574–6
[72] Chevallier J, Theys B, Lusson A, Grattepain C, Deneuville A and Gheeraert E 1998 Hydrogen-boron interactions in p -type diamond *Phys. Rev.* B **58** 7966–9
[73] Watanabe M O, Sasaki T, Itoh S and Mizushima K 1996 Structural and electrical characterization of BC2N thin films *Thin Solid Films* **281–282** 334–6